Observation of a transition state resonance in the integral cross section of the F+HD reaction

Rex T. Skodje, Dimitris Skouteris, David E. Manolopoulos, Shih-Huang Lee, Feng Dong, and Kopin Liu

Citation: The Journal of Chemical Physics **112**, 4536 (2000); doi: 10.1063/1.481041
View online: http://dx.doi.org/10.1063/1.481041
View Table of Contents: http://scitation.aip.org/content/aip/journal/jcp/112/10?ver=pdfcov
Published by the AIP Publishing

Observation of a transition state resonance in the integral cross section of the F+HD reaction

Rex T. Skodje
Institute for Atomic and Molecular Sciences, Academia Sinica, Taipei, Taiwan 106
and Department of Chemistry, University of Colorado, Boulder, Colorado 80309

Dimitris Skouteris and David E. Manolopoulos
Physical and Theoretical Chemistry Laboratory, South Parks Road, Oxford OX1 3QZ, United Kingdom

Shih-Huang Lee, Feng Dong, and Kopin Liu
Institute for Atomic and Molecular Sciences, Academia Sinica, Taipei, Taiwan 106

(Received 14 September 1999; accepted 8 December 1999)

We have studied the reaction F+HD at low collision energies using a combination of experimental and theoretical methods. Clear evidence for a reactive resonance is found in the integral cross section for the reactive channel F+HD→HF+D. Using a crossed molecular beam apparatus, the total reactive cross sections for the HF+D and DF+H channels were obtained in the collision energy range of 0.2–5 kcal/mol. In addition, Doppler profiles were obtained over this range of energies, which provide information about the angularly resolved distribution of final vibrational states. The cross section shows a distinctive steplike feature near 0.5 kcal/mol. Furthermore, the Doppler profiles reveal a dramatic change in the angular distribution of products over a narrow energy range centered at 0.5 kcal/mol. This feature is shown to arise from a reactive resonance localized near the transition state. Theoretical scattering calculations have been carried out using the Stark–Werner potential energy surface, which accurately reproduce the shape of the resonance feature. A detailed analysis of quantum dynamics using the spectral quantization method reveals that a quantum resonance exists near 0.52 kcal/mol, which is localized about the collinear FHD geometry. At collision energies below 1 kcal/mol, the reaction was found to proceed almost exclusively through resonant tunneling with very little contribution from direct, over the barrier, reaction. The properties of the quantum resonance, such as the position, lifetime, and partial widths were found to correlate well with the experimental results and the quantum scattering calculations.
 [S0021-9606(00)00709-1]

I. INTRODUCTION

The $F+H_2$ reaction has served as an archetypal system for the study of chemical reaction dynamics[1] and as a focal point in the search for reactive resonances.[2] A series of successive improvements in experimental and theoretical methods has led to a detailed understanding of many aspect of this reaction. Although this system has been studied for decades, much of the more recent interest in this problem was inspired by the crossed molecular beam experiments of Lee and co-workers.[3] An anomalous forward scattering peak in the state-resolved product distribution for $HF(v'=3)$ was observed at collision energies in the range, $E_C = 1.84-3.42$ kcal/mol, which seemed to provide evidence that reactive resonances may exist in this system. Additional molecular beam studies of $F+H_2$ and its isotopomers have subsequently provided higher levels of resolution and further details about the reaction and possible resonance features.[4] The evidence for reactive resonances in the beam experiments was not conclusive, however, since there are other dynamical explanations for the forward scattering peak when considered on the realistic potential surface.[5,6] Furthermore, the contemporaneous theoretical simulations could not reproduce the experimental results in a way that would confirm the existence of a resonance. Nevertheless, since this work, it has become the conventional wisdom that resonances should be sought in the differential cross section for collision experiments since impact parameter averaging is expected to smear out resonance features in the total reactive cross section.[7,8] This stands in contrast to resonances seen in, e.g., nuclear physics where strong resonant signatures are often apparent in the integral cross sections.[9] The issue seemed to be put to rest in the recent discussions of reactive resonances in the $H+H_2$ system where experiment[10] and theory[11] coalesced to show the resonances to be completely obscured in the integral cross section, $\sigma(E)$, but perhaps survived in the differential cross section, $d\sigma(E)/d\Omega$.

An alternative approach is to search for resonances using transition state spectroscopy, which is dynamically a half-collision process and circumvents the impact parameter-averaging problem. Neumark and co-workers[12] have recently observed the photodetachment spectrum of FH_2^-. The spectrum revealed structure, but, at the available level of energy resolution, the peaks could not be definitely assigned to transition state resonances.[6,13] Theoretical analysis assigned some of the spectral peaks to van der Waals type states or threshold type states[14] associated with the well in the long range entrance and exit channels but not to states trapped near the barrier. At this point in time, the only conclusive evidence for reactive resonances in bimolecular $A+BC$ reactions is for the I+HI system, which was studied by photodetachment of IHI^-.[15]

The theoretical investigation of $F+H_2$ reactive resonances has a long history, dating back to the collinear studies of Wu *et al.*[16] and Schatz *et al.*,[17] and since then a wide variety of dynamical methods and potential energy surfaces (PES) have been applied. In the simplest physical terms, the existence of reactive resonances was found to trace back to dynamical trapping in wells on the vibrationally adiabatic potential curves.[18] While a more sophisticated analysis is certainly possible, the vibrationally adiabatic model seems to provide the correct zero-order dynamical picture. The resonance energies are, of course, sensitive to the PES, and accurate predictions had to wait for a sufficiently accurate surface to be constructed.

Recently, a highly accurate PES has been developed by Stark and Werner (SW) (Ref. 19) that makes possible quantitative comparison with experiments. The SW-PES exhibits a highly bent saddlepoint and long range van der Waals wells in the entrance and exit channels. The dynamics on this PES has been studied using quasiclassical trajectory (QCT) simulations, by Aoiz *et al.*,[20] and also with full quantum scattering calculations, by Manolopoulos and co-workers,[6,21,22] and others.[23] The photodetachment spectrum of Neumark and co-workers has also been quantum mechanically simulated.[13,24] The comparison of the quantum simulation to the results of Lee and co-workers, while not perfect, was found to be reasonably good. The simulations of the FH_2^- photodetachment spectrum are also in fairly good agreement with experiment. These successes build confidence in the belief that the SW-PES is, in fact, sufficiently accurate to describe a variety of experimental observables.

While the SW-PES combined with accurate quantum mechanical simulations seemed to be getting close to the experimental observations, the role of transition state resonances was not totally clear. Using three-dimensional quantum simulations, Manolopoulos and co-workers[13,24] and Takayanagi and Kurosaki[26] have identified numerous resonance states trapped in the van der Walls wells for $F+H_2$, F+HD, and $F+D_2$, but not states localized near the saddlepoint. The van der Waals resonances are far too narrow to significantly affect the reaction probability and are probably not a good explanation for the results of Lee and co-workers although they probably influence the photodetachment spectrum. Of course earlier studies on other surfaces has yielded reactive resonances trapped near the saddlepoint.[25] While such resonances have not been reported on the SW-surface there is no reason to believe that they will not exist. Transition state resonances appear on all reasonable surfaces and appear to be quite robust with respect to details of the PES and dynamical approximation.

Manolopoulos and co-workers[6] and Takayanagi and Kurosaki[26] also have observed a broader peak, ''peak A,'' in the cumulative reaction probability for individual partial waves. For $J=0$, this peak lies at collision energy 0.4 kcal/mol in the $F+H_2$ reaction and moves steadily upward with the total angular momentum, J. The high J versions of this feature are apparently responsible for a large part of the forward scattering peak in the $HF(v'=3)$ product. Castillo and Manolopoulos have argued, based on a time-delay analysis, that peak A is not a resonance in the $F+H_2$ reaction, but is due to a kinematic tunneling effect.[6] An analogous peak was obtained in the F+HD reaction, which was tentatively attributed to the same sort of effect.[22] In this work, we shall reopen the interpretation of peak A for the F+HD case and come to the opposite conclusion.

In particular, we present an experimental and theoretical investigation of the reaction

$$\mathrm{F+HD}(v=0,j=0,1) \begin{array}{l} \rightarrow \mathrm{HF}(v',j') + \mathrm{D} \\ \rightarrow \mathrm{DF}(v',j') + \mathrm{H} \end{array}$$

at low collision energies, $E_C=0.2-5$ kcal/mol. There has been considerably less attention given to this isotope and to the low energy regime in particular. At such low energies, small features in the entrance channel of the potential energy surface may have a large effect on the reaction dynamics. Even if the van der Waals well does not trap resonance states, it still may significantly deflect incoming trajectories. Indeed, we shall observe a ''steering'' effect toward collision in the T-shaped geometry due to the long range potential. Low collision energies are also interesting since the number of partial waves contributing to the cross section is greatly reduced. Resonance features occurring at low energies may not be washed out to the extent seen at higher energies.

In the present work we return to the crossed molecular beam study of the reaction dynamics using an apparatus described in detail previously.[27] Due to technological improvements incorporated into the beam machine, it is possible to measure reliable cross sections to significantly lower collision energies than achieved in previous measurements on this system. In particular it is possible to go below the $HF(v'=3)$ energetic threshold which occurs at $E_C=1.1$ kcal/mol. Since theoretical calculations on various PES have predicted reactive resonances below the $v'=3$ threshold, it will be interesting to investigate this regime. Somewhat complicating the analysis of the results is the possible contribution of reaction involving the excited state atom, $F(^2P_{1/2})$. Since the excited state lies only 1.15 kcal/mol above the ground state $F(^2P_{3/2})$, there is no way to eliminate this species from the beam source. While reaction of F* with H_2 has been observed at low collision energies,[28] there is good reason to believe that the associated cross section is fairly small.[29,32] Consequently, we feel confident that the dominant contribution to the reaction at low energy occurs through the ground atomic state.

Our contention in this paper is that a feature seen in the integral cross section for F+HD is due to the existence of a reactive resonance. Since this assertion runs contrary to conventional wisdom, it is useful from the onset to state how the resonance might survive the averaging effects. In a sense, the result is consequence of some fortuitous features of the F+HD system. First, the resonance in question lies just above the entrance channel threshold. This minimizes the number of partial waves contributing at the lowest energies. Second, and most important, at the resonance energy there is little or no direct (or background) reactive scattering. All the reactive flux apparently passes through the resonance state. Thus, the integral cross section shows a sharp step, (roughly the low energy ''half'' of a Lorentzian) with a half-width equal to the resonance half-width. The half-Lorzentian can

be fit to the $J=0$ resonant reaction probability. At higher energy, but still below the direct reaction threshold, *J*-shifted resonances contribute to the cross section. However, these shifted Lorenztians combine to give a characteristic profile that is easily identifiable in the experimental cross section. Thus, although the resonance is *J*-shifted to higher energy, the absence of background reaction permits a direct analysis of the integral cross section.

Ultimately, the goal of both the experimental and theoretical analyses is a detailed understanding of the reaction process. By combining the experimental and theoretical investigations of this system, the hope is to provide a picture of the dynamical effects in this system. The work in this paper is divided into three components. First, the experimental measurements are carried out to identify potentially interesting phenomena. Second, quantum scattering calculations are performed to establish that the SW-PES combined with accurate quantum dynamics can reproduce the observed effects. And third, classical trajectory, wave packet, and spectral quantization calculation are employed to physically interpret the phenomena. All three components of this work are required to establish the existence of a reactive resonance.

In Sec. II, the experimental methods and results are presented. In Sec. III, the theoretical treatment of the reaction dynamics is presented. In the discussion in Sec. IV, the theoretical and experimental results are compared and the evidence in favor of the existence of a reactive resonance is summarized.

II. EXPERIMENT

A. Apparatus and method

The experiment was carried out in a crossed-beam scattering apparatus using the same procedures as described previously.[27] In brief, a skimmed F-atom beam was generated from a discharge source[30] of F_2 passing through a pulsed valve. The subsequent supersonic expansion translationally cooled the F-beam, which then collided with a target HD-beam from a second pulsed valve. By alternating the HD gas pulses and taking the difference signal, the H- or D-atom reaction product was interrogated using a $(1+1)$ resonance-enhanced multiphotom ionization (REMPI) detection scheme combined with time-of-flight mass spectrometry. One convenient feature of the apparatus is the ability to control the collision energy simply by changing the intersection angle of the two molecular beams without the need to change any other source parameter. Therefore, at a given intersection angle, the probe laser wavelength can be scanned and the resulting difference signals integrated over the entire Doppler profile to yield a quantity proportional to the integral reactive cross section. The reaction excitation function, i.e., the translational energy dependence of the reactive cross section, was then obtained by repeating the measurements at different intersection angles. To normalize the relative cross sections for the two isotopic channels, several back-to-back wavelength scans at fixed intersection angles were performed with appropriate measures taken to ensure that the H- and D-atom products were detected with equal efficiency. The resulting uncertainties in the relative cross section measurements were all within $\pm 5\%$ and the overall errors in the experiments (including uncertainties in the collision energy, as discussed below) were estimated to be less than $\pm 10\%$.

To span the collision energy range of this work ($E_C = 0.2-5$ kcal/mol), for each beam two different sources were employed. To produce the F-atom beam, a discharge was passed through 5% F_2 in either He or Ne at 8 atm. It is well known that a F-atom beam produced through a discharge contains significant amounts of the spin–orbit excited $F^*(^2P_{1/2})$ atoms.[28,31] However, there is experimental evidence that the reactivity of F* is, in fact, quite small compared to that of the ground state $F(^2P_{3/2})$ atom.[32] Thus, the results presented below should not be significantly affected by the negligibly small contribution from F*. To produce the target HD beam, either a reverse-seeded HD with $\sim 15\%$ Ar or the neat HD expansion was used. The beam speeds were determined by either the Doppler-shift or the fast ionization gauge measurement. Although the different beam sources cover different collision energy ranges, there are substantial intervals of overlap among them. The consistency of the steplike structure in the resulting excitation functions (see below) from different sets of source combinations confirms the accuracy of the speed determination and that the results are devoid of experimental artifacts after the density to flux transformation was implemented. The previous characterization of the neat expansion of the HD beam indicated an average rotational energy of 0.05 kcal/mol, which corresponds to a rotational temperature of 50 K with 82% in $j=0$ and 18% in $j=1$.[27] A similar, or somewhat colder, rotational distribution is anticipated for the reverse-seeded HD beam. The translational energy resolution of the experiment was governed by the velocity spreads and angular divergences of the two doubly-skimmed molecular beams. Near $E_C \sim 0.6$ kcal/mol, which is the region of interest of the report, the resolution was determined to be about 15% ($\Delta E_C/E_C$) while the uncertainty in absolute energy was less than 0.1 kcal/mol.

B. Results

Figure 1 shows the normalized excitation functions for the HF+D and DF+H product channels. The results of a previous QCT simulation on the SW-PES, presented by Aoiz and co-workers,[20] are also plotted for reference. It is clear that while there is reasonably good agreement for the DF+H channel, a very significant discrepancy between QCT and experiment is evident for the HF+D channel. The most striking observation of the experimental results is a pronounced steplike feature peaking at around 0.5 kcal/mol, which are completely absent in the QCT simulation. In view of the success of the SW-PES in predicting many other dynamical attributes for this and isotopically analogous reaction,[33] the discrepancy with the classical prediction suggests the quantal nature of this feature. Since the adiabatic barrier to reaction is about 1.0 kcal/mol on the SW-PES, the 0.5 kcal/mol feature in the HF+D channel must be mediated through tunneling, and must only produce $HF(v' \leqslant 2)$ product states.

The isotope branching ratio, $\sigma(DF+H)/\sigma(HF+D)$, observed in the experiment is qualitatively reproduced by the

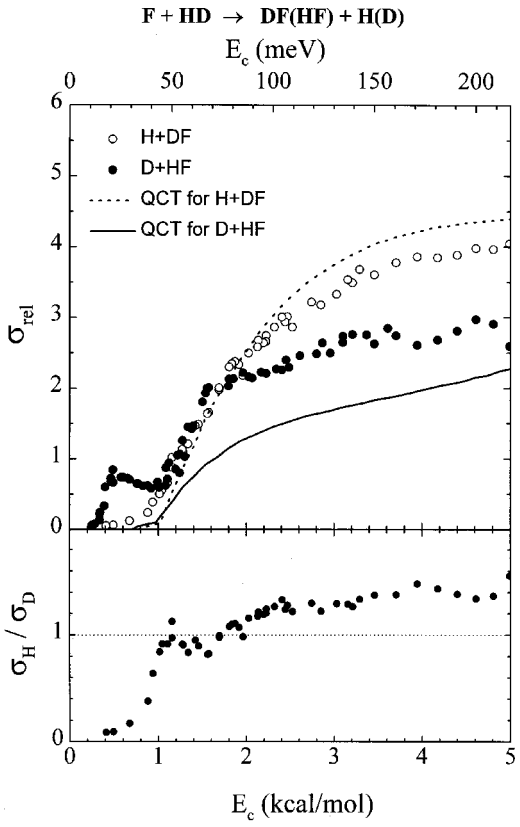

FIG. 1. The normalized excitation functions (upper panel) and the branching ratio (low panel) of the two isotopic channels for the F+HD reaction. The QCT simulations from Ref. 20 are plotted for comparison. The experiment is normalized to theory by a single scaling factor for both channels.

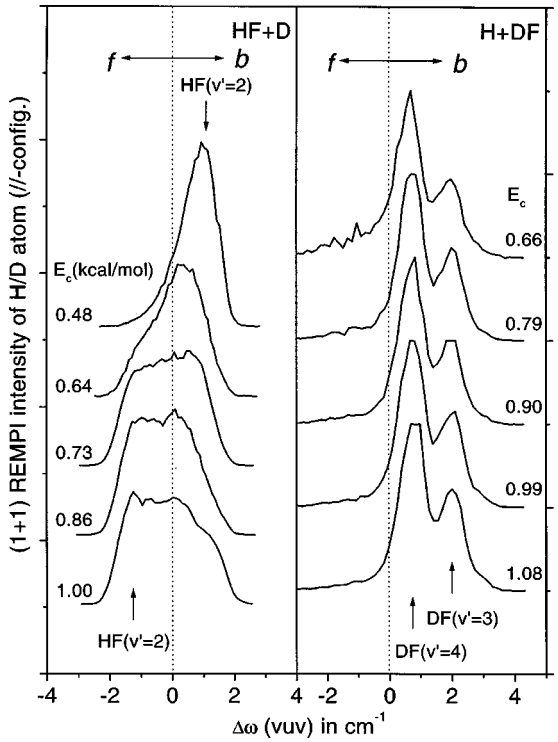

FIG. 2. A series of unnormalized ∥-Doppler spectra of the H/D-atom products taken for the two isotopic channels at tunneling energies. The shapes of these ∥-Doppler profiles provide an immediate view of the global angular distribution, as indicated by ''b'' (backward hemisphere) and ''f'' (forward hemisphere). Note the sharp contrast in product angular distributions for the two isotopic channels. Energetic considerations lead to the product vibrational state assignments of the observed features. These assignments are confirmed by the on-going c.o.m. differential cross section measurements.

QCT calculations at the higher energies. Thus, the propensity in favor of the DF product appears consistent with classical theory at these energies. The physical origin of the branching ratio may be similar to that seen in the Cl+HD reaction discussed recently.[34] At lower collision energies, the QCT branching ratio remains roughly constant while the experimental ratio decreases linearly in E_C except a ''bump'' near 1.2 kcal/mol. There are two identifiable features occurring at nearby energies that could be the cause of the bump, viz., either a threshold anomaly for the opening of the HF($v'=3$) channel or an effect of the adiabatic barrier to reaction. However, at this point the nature of this bump is unclear.

In addition to the facile control of collision energies in integral cross section measurements using this rotating source machine, further advantage can be taken to obtain differential cross section information as a continuous function of energy. A technique, referred to as Doppler-selected time-of-flight, has recently been developed and applied to a number of reactions[30,35,36] to directly map out the three-dimensional (3D) c.o.m. differential cross section. The first step of this new approach is the conventional (1D) Doppler-shift technique operated in the ∥-configuration, where the initial relative velocity of the colliding species lies along the propagation axis of the probe laser. It can readily be shown, and has been demonstrated previously,[37] that with the combination of energy conservation and the state-to-state probe, this 1D-projection measurement yields directly the product state-specific angular distribution. The kinematics of F+HD is particularly favorable to demonstrate the rich dynamical information using this simple technique with the rotating sources machine.

Plotted in Fig. 2 are a series of ∥-Doppler profiles of the D-atom product from the HF+D channel at energies in the vicinity of the 0.5 kcal/mol feature. The profiles begin predominantly backward peaked at 0.48 kcal/mol, then protrude into the forward hemisphere and become roughly isotropic at 0.73 kcal/mol (Ref. 38) and finally shift to a somewhat forward weighted distribution at higher collision energies. The dramatic evolution of the Doppler profiles over such a narrow energy range is truly startling and unprecedented. From the extent of the Doppler shift, all these Doppler features appear to arise mainly from the HF($v'=2$) product state. On-going experiments using the Doppler-selected TOF technique clearly demonstrate that this is indeed the case. The quantitative information on the rotationally state-resolved differential cross sections will be reported in the future. For comparison, a few ∥-Doppler profiles of the H-atom product from the DF+H channel in the threshold region are also shown in Fig. 2. By contrast, all the profiles now are nearly identical and display two backward peaks. Again, the Doppler-selected TOF measurements prove that these two peaks correspond to the DF($v'=4$) and DF($v'=3$) product states, respectively. A backward angular distribution confirms the previous study of this isotope channel at higher energies,[3] and is the expected behavior for a direct abstrac-

tion reaction with a rebound mechanism when viewed within the classical framework. The striking contrast between the vibrationally-specific angular distributions for the two isotope channels, seen in Fig. 2, strongly suggests that the 0.5 kcal feature might be a byproduct of the elusive dynamical resonance first predicted from the collinear model studies of this reaction over 25 years ago.[16,17] The theoretical investigation in the next section not only confirms this conjecture unequivocally, but also provides much deeper insights into the nature of the quasibound state.

III. THEORY

To help interpret the experimental findings, theoretical dynamics calculations have been performed in the low energy regime. The calculations were done on the SW-PES which does not explicitly include the spin–orbit coupling. The properties of the SW-PES have been discussed in detail elsewhere.[19] For convenience, here we review the characteristics of this PES specialized to the isotope F+HD and to the coordinate system we employ. For most depictions of the dynamics, we employed the α-channel Jacobi coordinates, (R,r,γ), where R is the F–$(HD)_{com}$ distance, r is the HD bond length, and γ is the angle between the R and r vectors. We define $\gamma=0°$ to the the FDH collinear arrangement and $\gamma=180°$ to be the FHD arrangement. The saddlepoints are located at bent geometries, $(R,r,\gamma)=(3.498,1.457,133.1°)$, in units of bohr and deg, for the FHD case and (3.186, 1.457, 53.3°) for the FDH case. The barrier height is 1.53 kcal/mol relative to the potential minimum in the entrance channel. The collinear barriers are located at $(R,r,\gamma)=(3.911,1.442,180°)$ for FHD and (3.431, 1.442, 0°) for FDH with a height of 1.92 kcal/mol. A normal mode analysis at the bent saddlepoints reveals that the reaction coordinate has large angular and translational components and relatively little vibrational, r, component. If the harmonic zero point energies of the vibration and bending modes are included, the adiabatic barrier height is 1.06 and 1.24 kcal/mol for FHD and FDH, respectively. The collinear configurations are unstable with respect to bending motion, since the collinear geometry is a local potential maximum vs γ, which suggests the collinear approach is dynamically unfavorable. In the entrance channel, a van der Waals well of depth 0.36 kcal/mol is located at the T-shaped geometry at $R=4.77\,a_0$. Thus, the long range part of the interaction should tend to steer the dynamics into a sideways approach. The important properties of the surface are summarized in Table I.

We have investigated the reaction dynamics for low energy F+HD collisions using a variety of theoretical techniques including converged time-independent scattering calculations, collisional wave packet dynamics, spectral quantization, and quasiclassical trajectories. Together, these approaches can provide insight in the reaction dynamics.

A. Reactive scattering calculations

In order to simulate the experimental results described in Sec. II, we have calculated the quantum mechanical cross sections for the F+HD reaction on the SW-PES. These calculations were performed using the same quantum reactive scattering methods used previously[22] to study this reaction at the collision energies investigated by Lee and co-workers.[3] It was a straightforward extension of this earlier work to perform the present calculations at more collision energies and for both quantum mechanical parity blocks so as to obtain the collision energy dependence of the cross sections for F+HD$(v=0,j=0)$ and F+HD$(v=0,j=1)$.[39]

TABLE I. Properties of SW-PES for F+HD.

Saddlepoint	R[a]	r[a]	γ[a]	V_0[b]	V_{ad}[c]
FHD-bent	3.467	1.458	131.6	1.53	1.06
FDH-bent	3.166	1.458	55.1	1.53	1.24
FHD-collinear	3.911	1.441	180	1.92	1.79
FDH-collinear	3.431	1.441	0	1.92	1.87

Normal modes[d]

Saddlepoint	ω_v	ω_{rxn}	ω_{bend}
FHD-bent	3216	*i* 714	227
FDH-bent	3294	*i* 526	276
FHD-collinear	3161	*i* 502	262
FDH-collinear	3347	*i* 474	231

Other properties

Exothermicity 31.32 kcal/mol					
r_e(HD)	1.400	r_e(HF)	1.735		
ω_0(HD)	3774	ω_0(HF)	4123	ω_0(DF)	2988
B_e(HD)	45.6	B_e(HF)	20.9	B_e(DF)	11.0
$E_{v=0,j=0}$(HD) 5.36 kcal/mol		$E_{v=3,j=0}$(HF)=38.32 kcal/mol			

[a]Jacobi coordinates expressed in units of bohr and deg.
[b]Energy expressed in kcal/mol measured relative to the minimum of the entrance channel well.
[c]Adiabatic barrier in kcal/mol computed using $V_{ad}=\hbar\Delta\omega_v/2+\hbar\Delta\omega_{bend}/2+V_0$ for the bent barrier and $V_{ad}=\hbar\Delta\omega_v/2+\hbar\Delta\omega_{bend}+V_0$ for the collinear barrier.
[d]The frequencies and rotation constants are in cm^{-1}.

The resulting cross sections for these two initial states of the HD-molecule are shown in Fig. 3, and the averaged cross sections simulating the experimental beam populations, 80% $j=0$ and 20% $j=1$ are compared with the present experimental results in Fig. 4. It is clear from the comparison that the simulation is in excellent agreement with experiment for the F+HD→DF+H reaction, and also in fairly good agreement with experiment for F+HD→HF+D. In particular, the distinct peak in the experimental F+HD→HF+D cross section at 0.5 kcal/mol is also very apparent in the simulation. However, this peak is somewhat larger in the simulation than in the experiment.

The discrepancy between theory and experiment presumably relates to inaccuracies in the SW-PES since the dynamical calculations are converged. The peak in the F+HD→HF+D cross section at 0.5 kcal/mol occurs below the classical threshold for the reaction, which has been determined to be around 1 kcal/mol in the QCT calculations on the SW-PES, and therefore involves quantum tunneling. Thus, we suspect that the SW-PES may permit too much tunneling. One source of error could be in the barrier height. Indeed, the adiabatic inclusion of spin–orbit coupling in the Hartke–Stark–Werner (HWS) surface[21] does predict an increase in the barrier energy by about 0.35 kcal/mol. A more detailed critique of the SW-PES will be deferred to Sec. IV. The tacit assumption from this point on will be that the SW-PES surface is sufficiently realistic, in spite of this discrep-

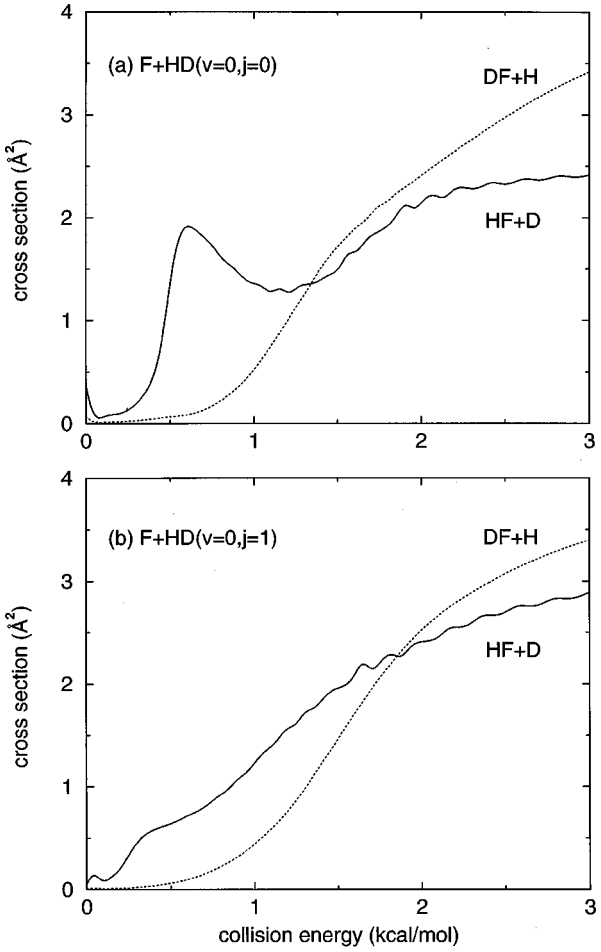

FIG. 3. Computed integral cross sections for the F+HD($v=0,j=0$) and F+HD($v=0,j=1$) reactions on the SW-PES vs collision energy.

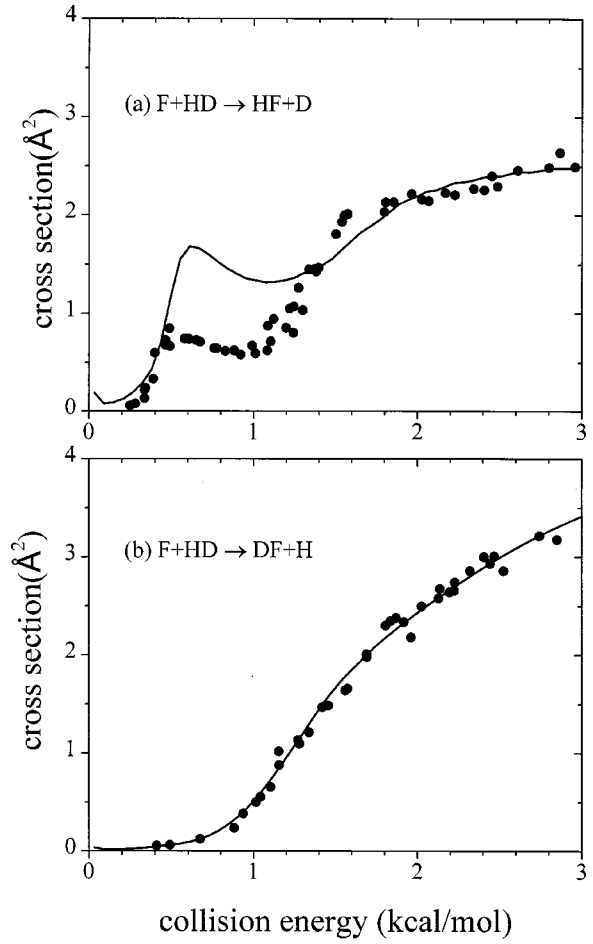

FIG. 4. Comparison of the computed cross sections for 80% HD($j=0$) and 20% HD($j=1$) with the experimental results multiplied by 8/9.

ancy, to give valuable insight into the experimental results present in Sec. II. In particular, we shall focus on the 0.5 kcal/mol peak in the F+HD($v=0,j=0$)→HF+D cross section in Fig. 4 and assume that whatever can be learned about this peak from the calculations applies equal well to the peak that is seen in the experiment.

One striking feature of the 0.5 kcal/mol peak that can be seen from Fig. 3 is that it is highly sensitive to the initial rotational state of the HD-molecule. The computed cross section for the F+HD($v=0,j=0$)→HF+D reaction shows the peak very clearly, but it is much smaller and shifted to lower energy in the cross section for the F+HD($v=0,j=1$) →HF+D. In order to investigate the peak further, we shall therefore concentrate exclusively on the F+HD($v=0,j=0$) →HF+D cross section, which is resolved into its partial wave (total angular momentum) components in Fig. 5. This resolution of the partial wave sum clearly shows the effect of partial wave averaging, which tends to ''smear out'' the peak in the integral cross section. The interesting thing is that the feature, although modified from pure Lorentzian, survives this averaging in both the experimental cross section measurement and the simulations.

Further insight into the origin of the peak can be obtained by using the data in Fig. 5 to plot the energy, E_J, of the peak maximum as a function of $J(J+1)$, as is done in Fig. 6. It is clear from this plot that the peak energy almost perfectly satisfies the equation one would expect for a linear triatomic. Furthermore, the rotational constant $B=0.0051$ kcal/mol that is obtained from Fig. 6 is too large to

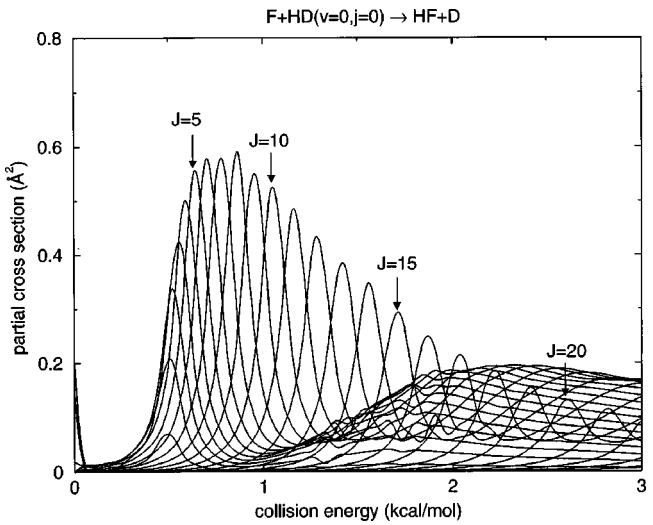

FIG. 5. Computed partial cross sections for the F+HD($v=0,j=0$) →HF+D reaction as a function of the total angular momentum quantum number, J, up to collision energies of 3 kcal/mol.

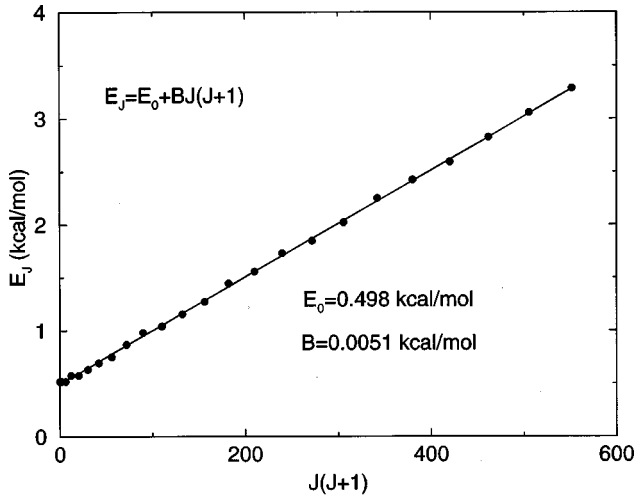

FIG. 6. The evolution of the energy, E_J, of peak A as a function of $J(J+1)$.

be consistent with anything other than a fairly compact geometry close to the transition state geometry of the reaction. Castillo and Manolopoulos[22] reached the same conclusion in an earlier study but were unable to determine whether or not the peak (referred to as peak ''A'' in Ref. 22) was due to a resonance. This issue will be settled conclusively in following sections, where we shall show that the peak is due to a quantum reactive scattering resonance with a collinear FHD geometry localized in the transition state region of the reaction.

B. Classical dynamics

A classical analysis of the reaction dynamics provides a useful complement to the quantum studies in two ways. First, the quasiclassical trajectories give us physical insight into the nature of the reaction coordinate. Second, a semiclassical treatment of the resonance using a periodic orbit analysis provides a useful approximation for the characteristics of the scattering resonance.

Aoiz and co-workers[20] have carried out a thorough QCT study of F+HD on the SW-PES. The results shown in Fig. 1 reveal that the experimental $\sigma(E)$ is in qualitative agreement with QCT at higher energies, especially for the DF+H channel. The 0.5 kcal/mol feature is not reproduced and is apparently a quantum mechanical effect mediated through tunneling. Nevertheless, the behavior of low energy trajectories gives some insight for dynamics in the entrance channel. In Fig. 7 we plot two quasiclassical ensembles with quantum numbers $v=0$, $j=0$, and $J=0$ in the coordinates (R,γ) (Ref. 40) at energies just below and just above the reaction threshold. Since vibrational adiabaticity in the entrance valley is essentially exact, the vibrational coordinate r is a spectator until the transition state is crossed. It is seen from the figure that the dynamics exhibits a very strong rotational-translational coupling. The collinear geometries, FHD and FDH, are seen to be very unstable with respect to rotational (bending) motion. Trajectories hitting the D-atom tend to be scattered toward the H-atom side while those impacting the H-atom are scattered toward the D-atom. Such trajectories

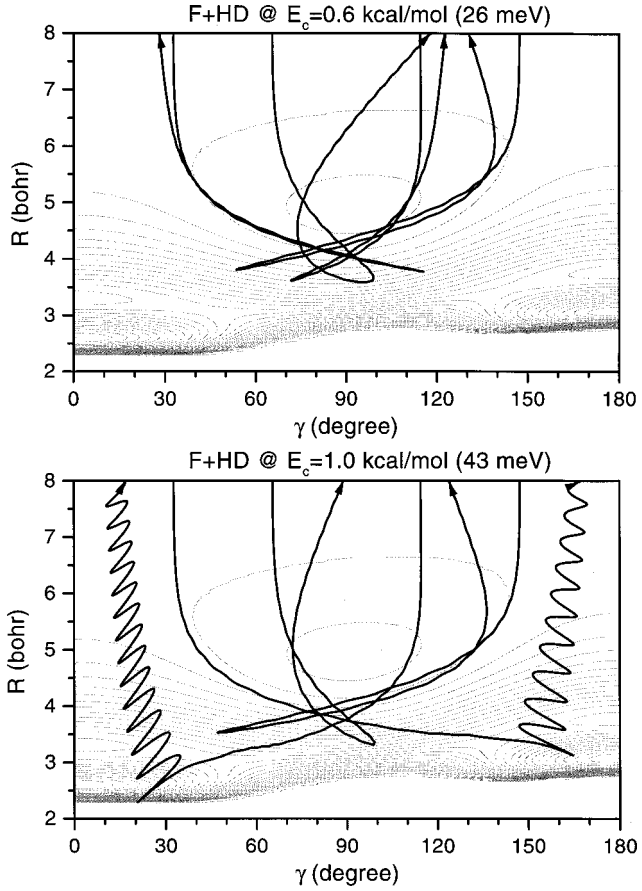

FIG. 7. Two ensembles of quasiclassical trajectories with $J=0$, $v=0$, and $j=0$ plotted in the (R,γ) coordinates. The top panel is at a translational energy of 0.6 kcal/mol, which is below the classical reaction threshold, while the lower panel is at $E_C=1.0$ kcal/mol, which is just above the reaction threshold.

were termed ''migratory'' by Aoiz *et al.*[20] As noted previously, addition of even one quantum of HD-rotational energy greatly suppresses the migratory reaction mechanism. During the ''internal rotation'' phase of these collisions, most of the kinetic energy resides in the rotational mode. Trajectories impacting near the T-shaped geometry, $\gamma=90°$, show little deflection and are never reactive. It is very interesting that almost all the reactive trajectories going into the HF+D channel first hit the D-atom, while for the DF+H channel they first hit the H-atom. Clearly, the reaction coordinate for passage over the transition state (especially into the HF+D channel) shows a very significant angular component. In this regard, the low energy F+HD collisions resemble those for the heavy–light–heavy system I+HI that show angular bottlenecks to reaction.[40,41] One can easily imagine that at collision energies below the classical barrier the reaction may occur by tunneling through an angular barrier initiated by a rotational scattering event.

A semiclassical treatment of reactive resonances can be obtained through the use of periodic orbits.[42] It has been observed that often a single orbit at the center of the classical complex region can provide reasonable predictions of resonance energies. For collinear resonance states, the so-called ''resonating periodic orbits'' (RPOs), first discussed by Pol-

lak and Child[43] have proved particularly useful. The quantization condition for the RPO is

$$\oint p \cdot dq = h(v_R + v_p + 1), \tag{1}$$

where (v_P, v_R) are quantum numbers for the exit and entrance channel ''local modes'' of the resonance. For asymmetrical reactions, the quantum numbers for which an actual quantum resonance exists generally corresponds to a situation of near degeneracy between the reactant and product local modes.[44] For the F+HD reaction, it is not obvious that the RPO's would prove useful in identifying resonances since the reaction path follows a bent geometry.

Using a Newton–Raphson search procedure, the RPO was found over a range of energies from slightly above the classical barrier to nearly the three-body dissociation limit. A quantized orbit in roughly the correct energy range and with an approximate degeneracy between the local modes was found to correspond to the quantum numbers $(v_P, v_R) = (3,0)$. This orbit was located using a numerical root search procedure with Eq. (1), was found to have an energy $E_C = -0.45$ (i.e., a total energy 4.91 kcal/mol), a period 22.5 fs, and Lyapunov numbers 4.73 and 0.24. Because the exit channel reaction path is strongly collinear, the RPO remains collinear. The orbit is shown later, in Fig. 14, along with a quantum resonance state of similar energy. Restricted to the collinear subspace, the RPO is stable at total energies above 9.3 kcal/mol. However, in three-dimensions the RPO is never stable which again points to the bending instability of the classical dynamics. Unlike for systems with a collinear reaction path, the local bending stability parameters of the RPO are not useful to obtain a bending frequency since the bend potential is a double well along much of the orbit. Instead, a bending frequency was obtained by time-averaging the bend potential, $V(\phi; R_{\mathrm{FH}}, R_{\mathrm{HD}})$, i.e., the full potential with the R_{FH} and R_{HD} bond lengths held constant, and the G-matrix element, $G_{\phi\phi}$, along the periodic orbit. Thus, we can use the quantities

$$V(\phi) = \frac{1}{\tau}\int_0^\tau V(\phi; R_{\mathrm{FH}}(t), R_{\mathrm{HD}}(t))dt,$$
$$G = \frac{1}{\tau}\int_0^\tau G_{\phi\phi}(\phi; R_{\mathrm{FH}}(t), R_{\mathrm{HD}}(t))dt \tag{2}$$

to define a semiclassical action and quantum number through

$$I(E) = \oint \sqrt{2(E - V(\phi))/G(\phi)}\, d\phi = h(v_{\mathrm{bend}} + 1/2). \tag{3}$$

The bend frequency was defined using the energy difference between the $v=0$ and $v=1$ solutions to Eq. (3), i.e., $E_1 - E_0 = \hbar\,\omega_{\mathrm{bend}}$. The result is $\omega_{\mathrm{bend}} = 320\,\mathrm{cm}^{-1}$. A prediction for the resonance energy in 3D can be made by adding the 2D RPO energy to the bending zero-point energy. The value obtained, $E_C = 0.46$ kcal/mol, is close to the 0.5 kcal/mol feature seen in the experiment and the quantum scattering calculation. We shall later see that a quantum resonance exists that is closely related to this classical orbit.

C. Collisional wave packet study

To investigate the dynamics at tunneling energies, it is necessary to adopt a quantum mechanical treatment of the reaction. Since the rotational (or bending) motion played a central role in the classical reaction mechanism, the use of a collinear or other two-dimensional representation of the reaction would be unwise. Therefore, we have carried out a three-dimensional time-dependent wave packet simulation for the case $J=0$. It is hoped that the dynamics of the lowest partial wave will be sufficient to gain a physical understanding of the dynamical effects at low energy.

The quantum wave packet calculations were carried out using a method described previously.[45] The following is a brief review. The system is described by the standard $J=0$ Hamiltonian for an $A+BC$ reaction expressed in Jacobi coordinates.[46] The wave function was represented on a spatial grid in the radial coordinates (R, r) and in a Legendre basis for the angular coordinate γ. Typically, the size of the representation (N_R, N_r, N_γ) is between (128,128,12) to (256,256,20). The wave packets were propagated using a Feit–Fleck split operator representation for the time-development operator, $U(\Delta t)$. The R and r contributions to kinetic energy are evaluated using fast-Fourier-transform (FFT) algorithm. The correct behavior at the origin is enforced using a sine-FFT representation. Using this propagator, the size of the representation is limited by the storage of $U(\Delta t)$, which consists of $N_R \times N_r$ matrices of size N_γ^2. The value chosen for Δt was 2 a.u.

Unphysical reflection of the wave packet at the edge of the grid was suppressed using an absorbing optical potential situated in the exit channels. A linear ramping form of the optical potential was used. The parameters were optimized to minimize reflection for each packet using analog collinear calculations as a guide. This was necessary since the low translation energy modes in the entrance channel are difficult to absorb.

The quantum dynamics of the low energy F+HD reaction can be visualized with the aid of quantum wave packets that propagate inward toward the barrier from the entrance channel. We have employed initial wave packets localized at R_0 in the entrance channel with average initial momentum $-P_0$ of a Gaussian form,

$$\Psi(R, r, \gamma, t=0) = \exp[-(R - R_0)^2/2\sigma^2 - iP_0 R/\hbar]\phi_0(r) L_j(\gamma). \tag{4}$$

Here, ϕ_0 is the ground vibrational eigenstate of HD and L_j is the jth-Legendre polynomial. The value of σ determines the energy dispersion of the packet. We wish to make σ large to minimize the spread around the mean collision energy, however it cannot be made too large without losing the physical insight into the reaction dynamics. In Fig. 8 we show snapshots of a wave packet with $j=0$, $\langle E \rangle = 0.6$ kcal/mol and $\langle \Delta E \rangle = 0.25$ kcal/mol at various stages of the collision process. For this wave packet, most of the reaction is due to tunneling. Two representations of the $|\Psi|^2$ are given; the first in the (R, γ) coordinates with r integrated out, and the second is a slice through the FHD collinear subspace, i.e., $\gamma = 180°$. At early times, the packet is uniformly distributed

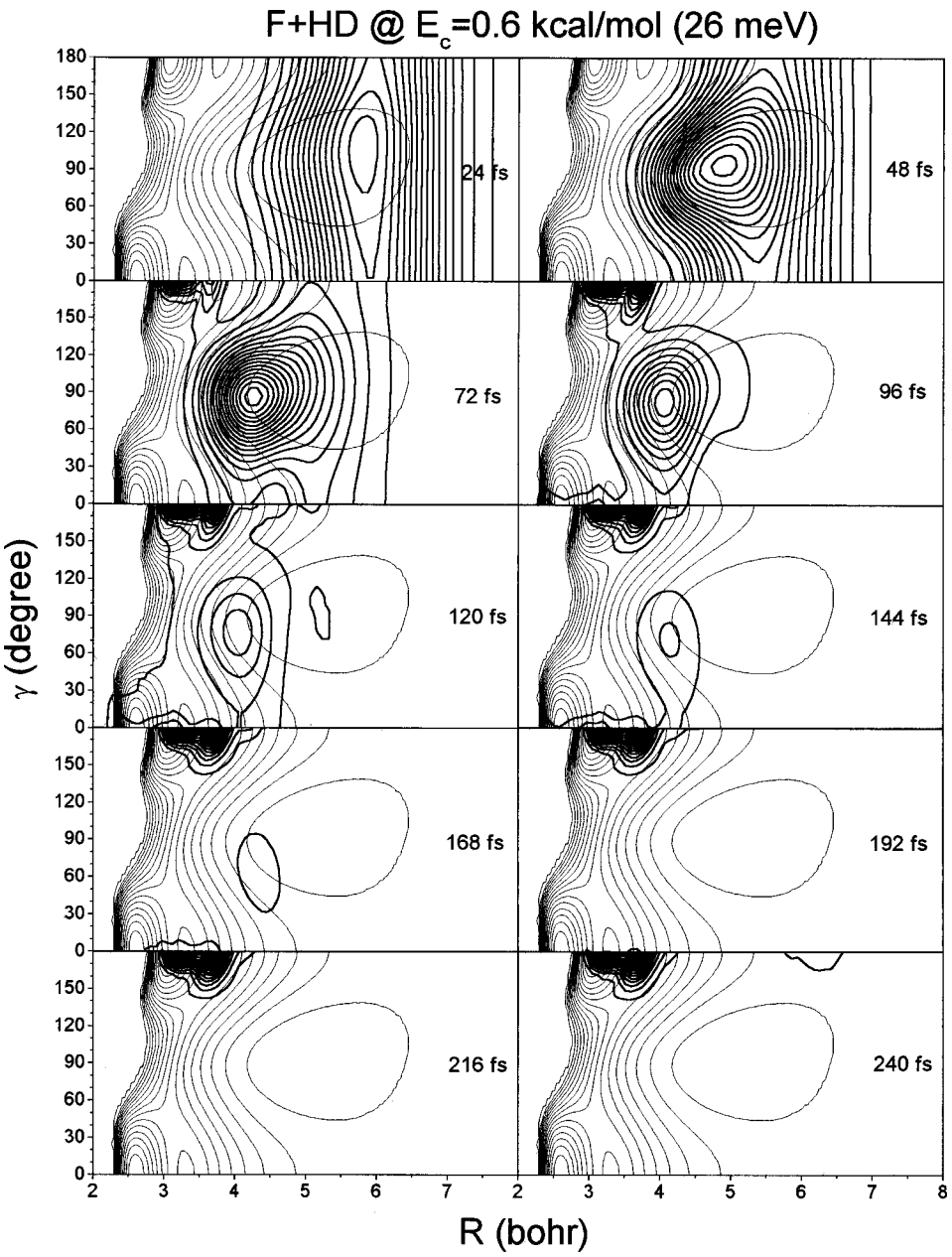

FIG. 8. Snapshots of a quantum wave packet started as a broad Gaussian in the F+HD($v=0,J=0$) channel with $\langle E_C\rangle = 0.6$ kcal/mol and $\Delta E = 0.25$ kcal/mol. The first set of panels show the packet in the (R, γ) coordinates with the r-coordinate integrated out. The second set of panels show the packet at the same times except in the FHD collinear subspace. The (R, γ) plots show the packet focusing into the T-shaped geometry and then tunneling through the barrier along an angular coordinate. The (R, r) plots show the creation of a persistent probability density near the transition state.

in angle, γ, and localized far from the barrier. As the packet approaches the barrier, the effects of the van der Waals well and of the collinear angular barriers tend to focus the wave packet into the T-shaped geometry, $\gamma = 90°$. This behavior is clearly reminiscent of the low energy classical dynamics. During the strong part of the collision, the packet spreads into the product wells mostly through the γ-coordinate motion. This angular tunneling path was also presaged from the classical mechanics. The density mainly enters into the HF+D reactive channel, with the much smaller DF+H contribution coming mostly from the higher energy tail of the wave packet. The collinear plots show the creation of a persistent density just past the saddlepoint with three plainly visible nodes. This density build up is localized at the collinear geometry showed no nodes in the γ-direction. This density pattern persists out to the longest times in the simulations. The results of this simulation are consistent with the collisional formation of a reactive resonance with a linear geometry.

We have also considered collisions with $j=1$, which make about a 20% contribution in the experiment. The essential difference with the $j=0$ dynamics seems to trace back to the $\gamma = 90°$ node in the initial wave function for $j=1$. This node, which persists during the evolution, inhibits the focusing of the wave packet at the T-shaped geometry and, hence, the subsequent angular spreading into the reactive channel. However, one still observes the formation of a three-node amplitude in the FHD linear arrangement, but there is much more reflection of the packet back into the F+HD entrance channel. The ratio of reaction probabilities at $\langle E\rangle = 0.6$ kcal/mol, $P(j=0):P(j=1)$, is about 2.5:1, which is consistent with the results of the scattering calcula-

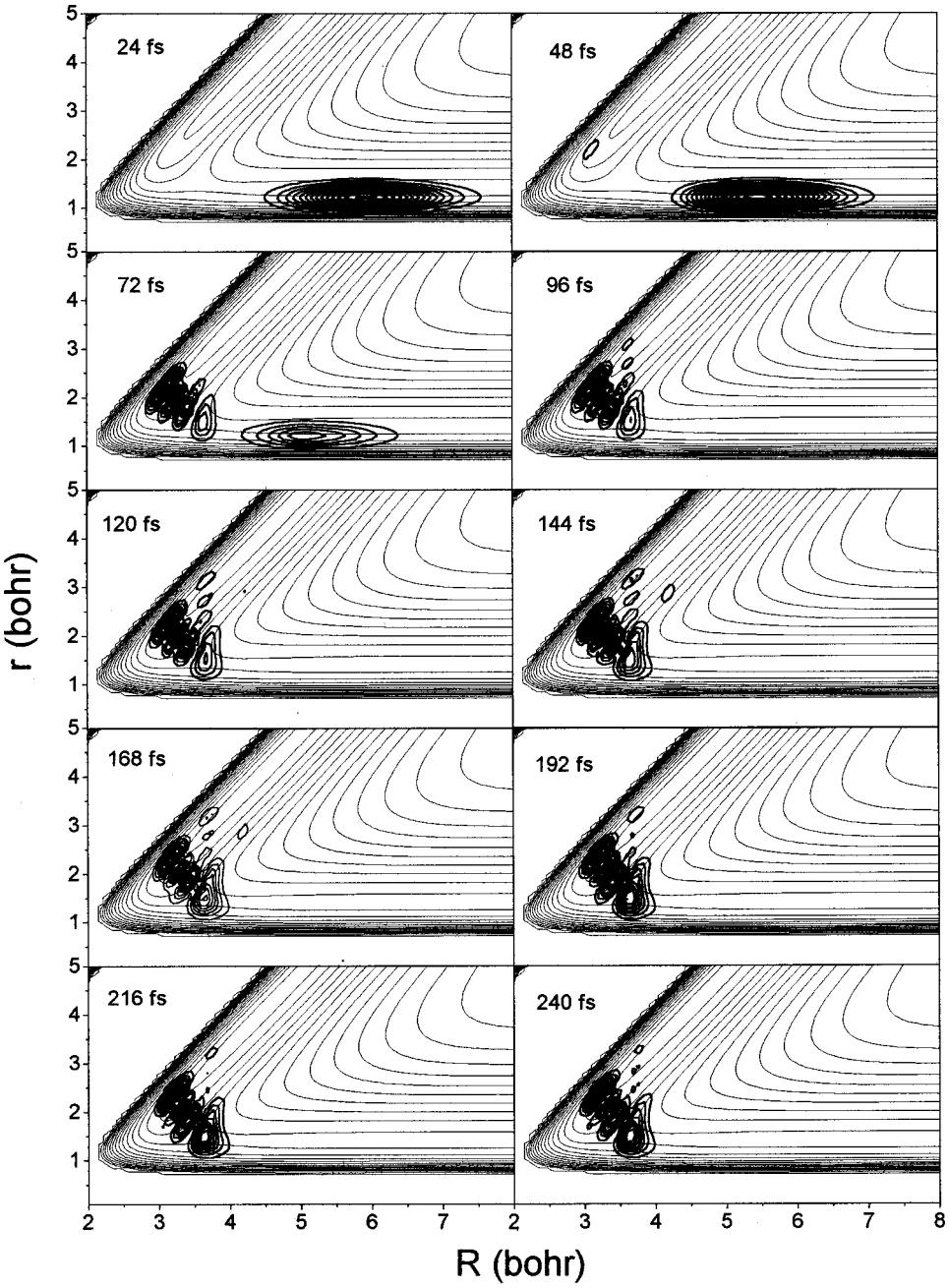

FIG. 8. (*Continued*.)

tion presented above when averaged over the energy spread of the packet.

D. Spectral quantization

To investigate the possibility of a reactive resonance near 0.5 kcal/mol, we have carried out an analysis of the reaction using the spectral quantization (SQ) procedure.[14,45,47,48] The transition state was probed using a set of initial wave packets propagated from near the saddle-point. Background was reduced by optimization of the initial packet. Using a control algorithm described previously, the spectral background was minimized using an initial state obtained variationally from the sum of five Gaussian basis functions localized at points near the collinear FHD RPO. A typical spectrum (using an unoptimized initial packet) is shown in Fig. 9. The intense peak at $E_C = 0.52$ kcal/mol is a candidate for the reactive resonance. The wave function associated with this peak was extracted from the optimal wave packet using the Fourier transform

$$\Phi_{\mathrm{res}}(R,r,\gamma) \propto \int_{-\infty}^{\infty} \Psi(R,r,\gamma,t) \cdot e^{iE_{\mathrm{res}}/\hbar} dt. \tag{5}$$

The probability density for the resonance wave function is shown in Fig. 10. It is seen to have the same nodal pattern as the state created in the collisional wave packet study, namely three-nodes in the asymmetric stretch direction and zero-nodes in the bending and symmetric stretch directions. To further verify that this state is a resonance, we have propagated numerous packets that show a peak fixed at this energy with similar linewidths. Final, convincing evidence of the resonance character of this state was obtained using a time decay calculation. The resonance wave function pictured in

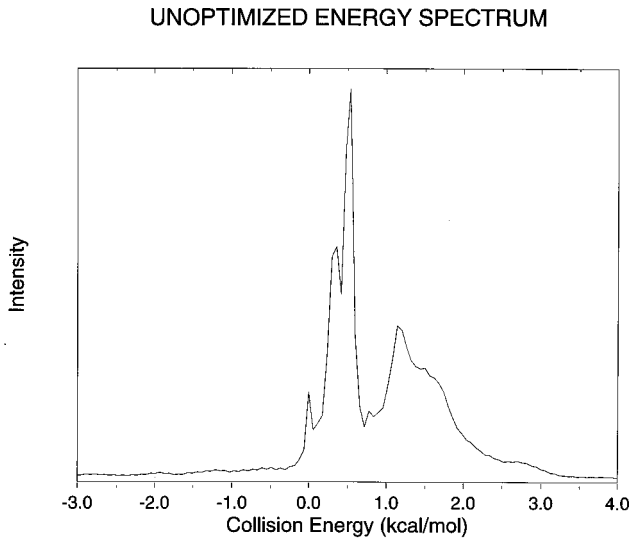

FIG. 9. A typical energy spectrum employed by the spectral quantization method that is used to identify resonance states.

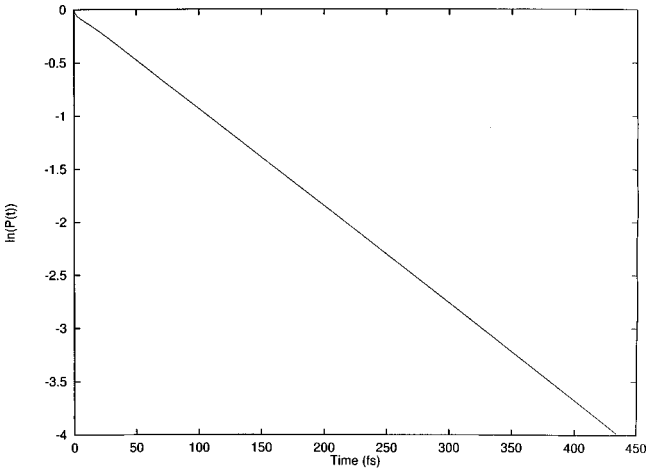

FIG. 11. The natural logarithm of the survival probability of the resonance state shown in Fig. 10 as a function of time. The figure clearly shows an exponential decay after an induction period.

Fig. 10 was used as an initial state for a new wave packet calculation. The decay of the survival probability, plotted in Fig. 11, shows exponential decay after an induction period. As discussed in our previous work, the induction period of slower decay is due to the existence of incoming waves in the Fourier extracted wave function. When the incoming wave is depleted, pure exponential decay is established. The lifetime obtained from the decay calculation is 109 fs. This value is consistent with the lifetime obtained by a Lorenztian fit to the spectral peak shown in Fig. 9. It is also consistent with the linewidth of peak ''A'' from the scattering calculations.

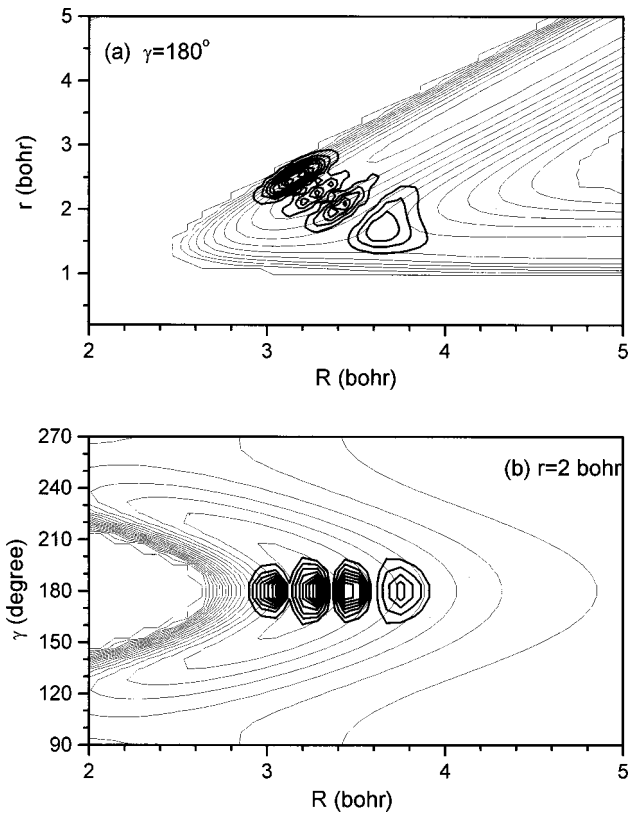

FIG. 10. The probability density of the reactive resonance at $E_C = 0.52$ kcal/mol. In the top panel the FHD collinear subspace is shown using the coordinates (R, r). In the bottom panel, the probability density is sliced at $r = 2$ bohr and is shown in the (R, γ) coordinates. The plot clearly shows a state with three-nodes along the asymmetric stretch and zero nodes in the symmetric stretch and bend.

The branching ratios of the decay products, F+HD($v' = 0, j'$) and HF(v', j')+D are calculated by computing the decay flux projected onto the various exit channels. The flux into the DF+H reactive channel was very small and was not accurately measured. To obtain the branching ratios in the HF(v', j')+D channels it was necessary to switch to the D+HF channel Jacobi coordinates. Unlike time-independent calculations, for the time-dependent decay of an unstable state the flux into the decay channels has an intrinsic dependence on the translational coordinate R at which the flux is evaluated.[49] Effectively, the flux at a value R depends on the decay rate of the resonance at an earlier time, $t = R/v$, where v is the channel velocity. Thus, due to this retardation effect, the flux increases with R since the resonance has a greater population at earlier times. This R-dependence can be eliminated by multiplying the flux by $\exp(-R/v\tau)$, which is consistent with the continuity equation for an exponentially decaying state with lifetime τ. As an illustration, in Fig. 12, the flux into each HF (v') product vibration state is plotted vs time and the rotational channels have been summed over. The final results, shown in Table II, indicate that the resonance decays into both the nonreactive and reactive channels but shows a strong preference for the FH+D reactive channel. The vibrational product distribution is dominantly into the FH ($v' = 2$) channel, with a probability of 97%. The HF ($v' = 1$) channel has a 3% probability and HF ($v' = 0$) is ~0.1%. The rotational distributions are somewhat more difficult to numerically converge due to need to represent the dynamics further into the exit channels. In the F+HD channel, the branching ratio, $P(j=0)$: $P(j=1)$ is 2.4:1. The $j = 2$ state is energetically closed at the resonance energy. The rotational distribution for decay into the HF ($v' = 2, j$)+D

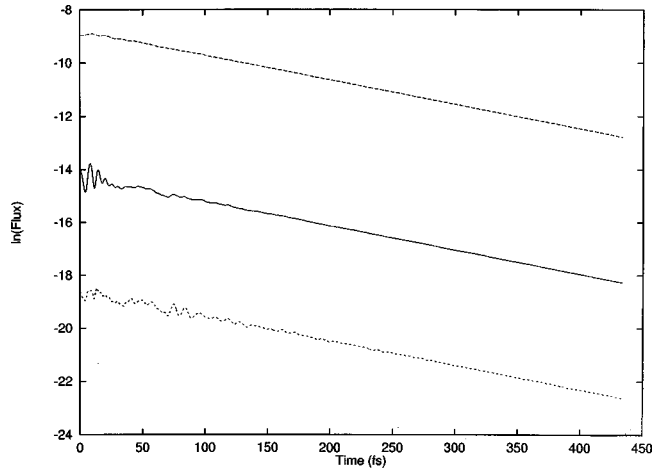

FIG. 12. The natural logarithm of the quantum flux into the vibrational channels HF($v'=2$), HF($v'=1$), and HF($v'=0$) as a function of time. The fluxes show exponential decay corresponding to the lifetime of the state. The flux is divided by the survival probability and corrected for the channel radius to obtain the branching ratios report in Table II.

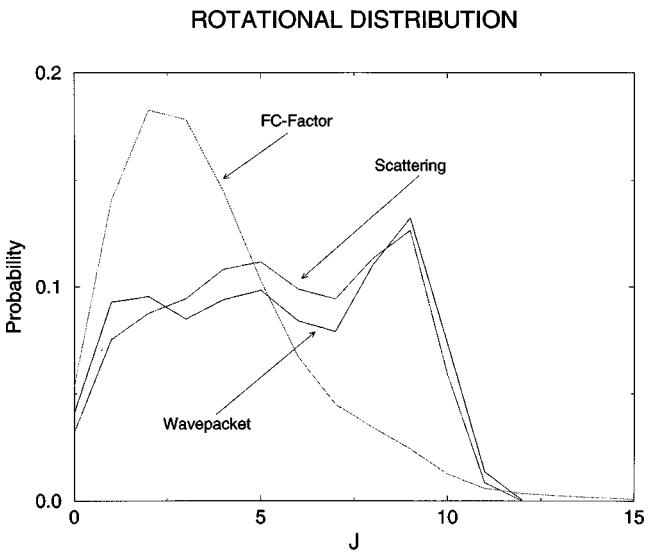

FIG. 13. The resonance decay probability into the rotational channels HF($v'=2,j'$) and the Franck–Condon factors of the resonance state. The curve marked ''wave packet'' is the asymptotic normalized decay probability projected onto the HF($v'=2,j'$) rotational channels. The curve marked ''scattering'' was obtained from the *S*-matrix $S(v=0,j=0;v'=2,j')$ at $E_C=0.6$ kcal/mol. The ''FC-factor'' curve was obtained by projecting the resonance wave function unto the asymptotic rotational states of HF.

channels, shown in Fig. 13, is seen to be extremely broad. The average rotational energy release is about 3 kcal/mol, which is nearly a third of the available energy in the $v'=2$ channel. The $J=0$ scattering calculations at 0.6 kcal/mol also exhibit a similar distribution of rotational populations as shown in the figure.

The very hot rotational distribution of the HF-product might, at first sight, be simply attributed to the rotational Franck–Condon factors of a linear-triatomic to atom+diatomic free rotor decay process for the resonance.

TABLE II. Theoretical characteristics of transition state resonance.

3D($J=0$)	
E_{res}	5.88 kcal/mol
$E_C=E_{\text{res}}-E_{v=0,j=0}$(HD)	0.52 kcal/mol
Lifetime	109 fs
B_0	1.8 cm^{-1}
Vib. branching ratios (HF+D)	HF($v'=2$)=0.97, HF($v'=1$)=0.03, HF($v'=0$)=0.001
Rot. branching ratios (F+HD)	HD($j=0$)=0.7, HD($j=1$)=0.3
Channel branching ratios	(HF+D)=0.6, (F+HD)=0.4, (DF+H)$\leqslant$0.01
Quantum numbers (local mode picture)	$v_{\text{FH}}=3$, $v_{\text{HD}}=0$, $v_{\text{bend}}=0$
Quantum numbers (normal mode picture)	$v_{\text{as}}=3$, $v_{\text{ss}}=0$, $v_{\text{bend}}=0$
Bending frequency=E_{res}(3D)−E_{res}(2D)	349 cm^{-1}
Collinear	
E_{res}	4.88 kcal/mol
$E_C=E_{\text{res}}-E_{v=0}$(HD)	−0.48 kcal/mol (below threshold)
Lifetime	1300 fs
Product branching ratios	HF(2)=0.91, HF(1)=0.09, HF(0)=0.003
E_{res} (semiclassical)	4.91 kcal/mol
B_0 (semiclassical)	1.62 cm^{-1}
Bend frequency (semiclassical)	320 cm^{-1}

However, we have computed the FC-factors by projecting the asymptotic free-rotor states onto the resonance wave function, and the result is not nearly so broadly distributed. As shown in Fig. 13, the FC-factors also fail to account for the peaking at $j'=9$. We believe the broad and inverted rotational distribution is further evidence of the strong role of rotational (or bending) motion in the reaction dynamics. The decay of the resonance state has major contribution from bending dynamics, as did the collisional formation of the reactive complex. Angular tunneling into the high-j' states may be an important effect.

The rotational properties of the triatomic complex can be investigated by computing the rotation constant B_0 for the resonance state. Based on the assumption of a linear complex, B_0 was computed by taking the expectation value of the inverse moment of inertia with the resonance state, and then

$$B_0=\frac{\hbar^2}{2}\left\langle\frac{1}{I}\right\rangle. \tag{6}$$

Since we do not want to include the contribution from the decay products, the integration in the matrix element is cut-off beyond $R=4\,a_0$. The result is $B_0=1.8\,\text{cm}^{-1}$. This is close to the value of 1.62 cm^{-1} obtained classically by time-averaging the moment of inertia along the quantizing periodic orbit. It is also identical to the value $B_0=0.0051\,\text{kcal/mol}=1.8\,\text{cm}^{-1}$ obtained from the *J*-dependence of peak ''A'' in the scattering calculations.

Although the resonance at 0.52 kcal/mol is our primary interest since it serves as an explanation for the peak in the cross section, for completeness we have also located several other transition state resonances that lie outside of the energy range of interest. In the FHD collinear configuration, we have found resonances at $E_C=9.25$ and 11.50 kcal/mol.

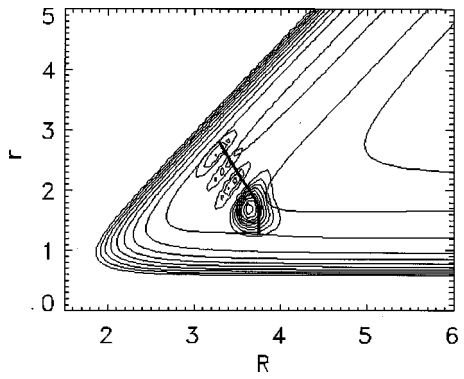

FIG. 14. The probability density for the (3, 0) resonance of the collinear F+HD reaction. The quantizing periodic orbit, RPO, is overplotted on the wave function.

These resonances are also spatially localized in the region of the transition state with 1 node along the HD coordinate and 4 (and 5) nodes in the FH coordinate. In the FDH arrangement, a resonance was found at $E_C=-0.46$ kcal/mol with four-nodes in the FD coordinate, zero-nodes in the HD coordinate, and zero-bending nodes. We also identified resonance states at $E_C=0.3$, 1.1, and 1.6 kcal/mol which are the previously discovered[22,26] ''uninteresting'' resonances located in the channel wells.

To label the resonance states, it is necessary to adopt a zero-order reference system that mimics the dynamics near the transition state. Several schemes are possible. One might use the vibrational states of a linear triatomic molecule using local or normal modes. Alternatively, hyperspherical modes have been proposed to model heavy–light–heavy type systems. Here, we find it convenient to use a local mode description, which was used previously for $D+H_2$.[44] For the FHD collinear arrangement, we can use the quantum numbers $(v_{\mathrm{FH}},v_{\mathrm{HD}},v_{\mathrm{bend}})$ and for the FDH arrangement, $(v_{\mathrm{FD}},v_{\mathrm{HD}},v_{\mathrm{bend}})$. In this scheme, the resonance at 0.52 kcal/mol is (3, 0, 0). The resonances at 9.25 and 11.50 are (4, 1, 0) and (5, 1, 0). The resonance at -0.46 kcal/mol is the (4, 0, 0) state referenced to the FDH geometry.

Since the resonance states we have obtained are localized in the FHD linear geometry, it is useful to consider the collinear version of the reaction on the SW-PES. We have previously investigated[14] the collinear dynamics of $F-H_2$ on the SEC6-PES of Truhlar and co-workers[50] and so here we merely redo similar calculations on a different surface. The analogous resonance state for the collinear reaction is found below the F+HD threshold at $E_C=-0.48$ kcal/mol ($E_{\mathrm{total}}=4.88$ kcal/mol), which is quite close to the value predicted by the RPO. The resonance wave function, shown in Fig. 14, is similar in appearance to the collinear slice of the 3D state pictured in Fig. 10. The RPO, also pictured here, is seen to lie in the region of high probability density. If the energy difference between the 2D and 3D states is interpreted as due to bending zero point energy, i.e.,

$$E_{\mathrm{res}}(3\mathrm{D})=E_{\mathrm{res}}(2\mathrm{D})+\hbar\omega_{\mathrm{bend}}, \tag{7}$$

then the bending frequency is 349 cm^{-1}, close to the result obtained semiclassically. The lifetime of the collinear resonance, obtained from the exponential decay rate of a prepared resonance state, was found to be quite long, 1.3 ps, more than an order of magnitude larger than the 3D result. This makes clear once again that the bending instability of the dynamics plays a major role in the decay of the resonance. The branching ratio of HF(v') products was similar to the 3D case although the $v=0,1$ probabilities are three times higher for the collinear case.

IV. DISCUSSION

The exhaustive study of the $F+H_2$ reaction and the recent successes of quantum dynamical simulations had led to the speculation[51] that the last chapter had been written on the nature of the FH_2 transition state. In this work, perhaps an appendix has been added to this volume of research. We believe that the sort of reactive resonance inferred by Lee and co-workers, and analyzed through many theoretical studies, has finally been observed in a beam experiment. The remarkable aspect of this discovery is that the resonance survives in the integral cross section. It is a fortunate accident that the resonance for the F+HD isotope lies so near the threshold that direct reaction does not appear to interfere with the resonant scattering. The reaction mechanism at low energies is essentially pure resonant tunneling which gives rise to a distinctive excitation function even when averaged over an angular momentum. In this section, we shall explore the nature of a resonance-mediated reaction in more detail, and attempt to correlate the results obtained theoretically and experimentally. We shall argue that all the experimental findings are consistent with the view that the reaction near $E_C=0.5$ kcal/mol is mediated through a reactive resonance and that for $E_C>1.1$ kcal/mol the reaction becomes increasingly dominated by over the barrier dynamics and the opening of the HF($v'=3$) channel.

A. Resonance mediated reaction

For a resonance-mediated reaction, the reaction proceeds by the collisional formation of a resonance and subsequent decay into product channels. This sort of mechanism is visualized through the wave packet evolution shown in Fig. 8. Unlike other systems, which may have reactive resonance but usually at energies above the barrier energy, for F+HD there is no direct contribution to the reactive cross section at low energies. The resonance thus serves as a ''gateway-state'' and, in fact, the only pathway through which all the reactive flux must pass. Such a reaction mechanism was implicit in the studies of collinear $A+BA$ model systems by Bisseling *et al.*[52] In a resonance mediated reaction many of the characteristics of the reactive cross section can then be tied to the properties of the resonance. Specifically, the resonance energy, width, and partial widths can be used to characterize the full reaction dynamics at low energies. Furthermore, at sufficiently low temperatures the thermal rate constant will be dominated by the resonance contribution to the reaction.

B. Reactive cross sections

We first consider the issue of the influence of an isolated near-threshold resonance on the excitation function. A reso-

nance has not been seen in an integral cross section for a chemical reaction before, and it is have often been argued that resonances will not be observed in the integral cross sections because of the effect of partial wave averaging. It is therefore interesting to investigate the resonance contribution to the computed F+HD→HF+D cross section in a little more detail. The most effective way we have found to do this is to combine the expected resonance contribution to the reaction probability at $J=0$ with the usual J-shifting approximation.[53] The reaction probability going from the α-channel to the β-channel is

$$P_{\alpha\to\beta}(E,J=0)=\text{const}\cdot\frac{\Gamma_\alpha\Gamma_\beta\sqrt{E_\alpha}\sqrt{E_\beta}}{(E-E_{\text{res}}(J=0))^2+\Gamma^2/4}, \quad (8)$$

where E_α and E_β are the channel translational energies and Γ_α and Γ_β are the partial widths of the resonance, which satisfy $\Sigma\Gamma_\gamma=\Gamma$. Equation (8) is the Breit–Wigner expression for the contribution from a single pole in the S-matrix at $E_{\text{res}}-i\Gamma/2$, although usually the kinematic energy factors are assumed to be constant over the width of the resonance. However, it is known that for near-threshold resonances one term should be retained for low translational energy.[9,40] When this expression is combined with the standard J-shifting approximation to the cross section,

$$\sigma_{\alpha\to\beta}(E)=\frac{\hbar^2\pi}{2uE_\alpha}\sum_{J=0}(2J+1)P_{\alpha\to\beta}(E-B_0J(J+1), \quad J=0), \quad (9)$$

we obtain the resonance contribution to the cross section. The resonance parameters required in this formula may be obtained either from the spectral quantization results or from a fit to peak A in the $J=0$ scattering calculation; and both methods yield nearly equal results. For definiteness, we opt to fit peak A. The top panel of Fig. 15 shows the fit obtained to the $J=0$ reaction probability using Eq. (8) with E_β assumed constant, and bottom panel shows the corresponding resonance contribution to the integral cross section. The resonance parameters obtained were $\Gamma=0.148$ kcal/mol, $E_{\text{res}}=0.498$ kcal/mol, and $B_0=0.0054$ kcal/mol$=1.9\,\text{cm}^{-1}$. In Fig. 15 we plot the resonance contribution to the cross section along with the calculated cross section. Below about 1 kcal/mol, it is seen that this expression reproduces nearly exactly the calculated cross section and also the shape (but not the magnitude) of the experimental excitation function. The clear message from the bottom panel of the figure is that the resonance survives partial wave averaging to appear as a distinctive feature in the integral cross section because it occurs so far below the classical threshold for the reaction. From this analysis we can conclude that the 0.5 kcal/mol in the experimental cross section is in fact the resonance contribution.

The calculated cross section for F+HD($v=0,j=1$) shown in Fig. 3 also shows a steplike feature at low energy but is not so distinct as for the $j=0$ case. We can use Eq. (8) to compute the resonance contribution to this process as well. The only difference with the previous $j=0$ analysis is an overall factor of the partial width appropriate to each channel and an energy shift ΔE equal to the rotational spacing of HD. The energy level spacing between $j=0$ and $j=1$ is 0.26 kcal/mol which is, in fact, equal to the peak shift between the two cross sections seen in Fig. 3. The ratio of peak heights is roughly 3:1 which is close to the ratio of partial widths, $\Gamma(\text{F+HD}(v'=0,j'=0))/\Gamma(\text{F+HD}(v'=0,j'=1))=2.5$, when the translational energy factor in Eq. (8) and the helicity are taken into account.

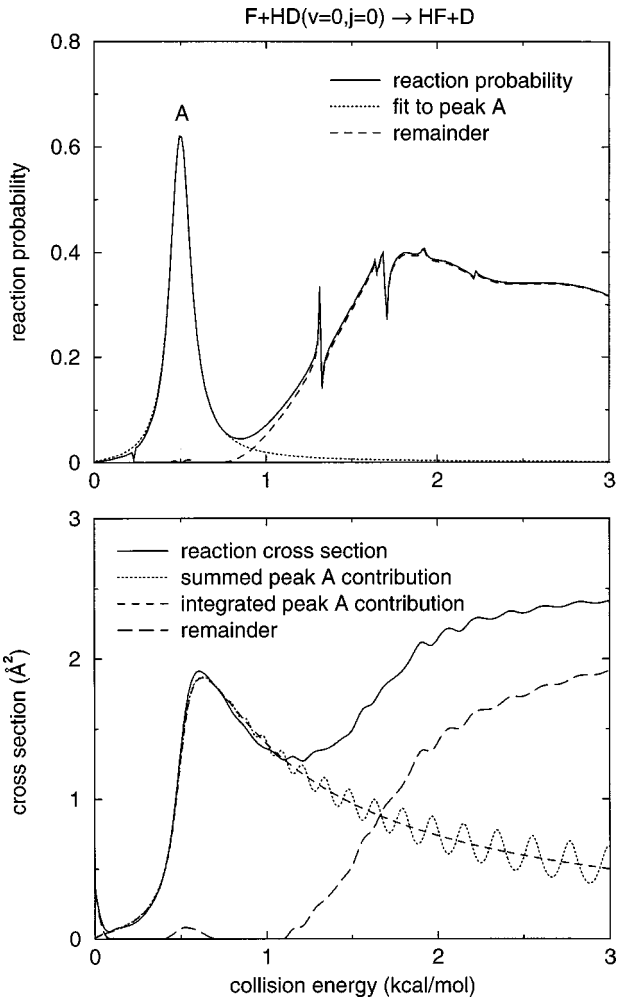

FIG. 15. Analysis of the contributions of peak A to the computed $J=0$ reaction probability [top panel, see Eq. (8)], and to the integral cross section [bottom panel, see Eq. (9)] for the F+HD($v=0,j=0$)→HF+D reaction. In fitting the resonance peak, the exit channel velocity term was held fixed.

We note the small oscillations evidenced in the calculated cross sections in Fig. 3 at energies above 1 kcal/mol. Comparing Fig. 3 to the bottom panel of Fig. 15 suggests that the small oscillations from the high-J resonance terms in Eq. (9). Indeed, a comparison between the spacing in the oscillation with the spacing between the J-shifted versions of peak A is consistent with that view. The experimental excitation function is not resolved to the point where such small oscillations might be detected.

The remaining, nonresonant, contribution to the theoretical F+HD→HF+D cross section is seen, in Fig. 15, to show a typical threshold type behavior between 1 and 2 kcal/mol. A similar threshold is observed in the case F+HD→DF+H, which of course has no resonance contribution at low energy. This pattern is consistent with the onset

of direct reaction at collision energies higher than the adiabatic barrier height. The experimental F+HD→DF+H cross section threshold agrees almost perfectly with the results of the scattering calculation. For the F+HD→HF+D reaction over the same energy range, the experimental cross section deviates slightly from the theoretical prediction in shape, but still seems consistent with a direct reaction threshold.

Finally, we note that if the resonance cross section, Eq. (9), is evaluated using the classical approximation that the *J*-sum can replaced with an integral, an analytical expression may be obtained,

$$\sigma_{\alpha\to\beta}(E)=\text{const}'\cdot\frac{\Gamma_\alpha\Gamma_\beta}{B_0\Gamma\sqrt{E_\alpha}}\text{Im}\left[\theta(E_\alpha)\ln\left(\frac{\theta(E_\alpha)+1}{\theta(E_\alpha)-1}\right)\right], \tag{10}$$

where

$$\theta(E_\alpha)=\sqrt{\frac{(E_{\text{res}}(J=0)-i\Gamma/2)}{E_\alpha}}. \tag{11}$$

It is interesting to note that in this approximation the value of B_0 only enters the cross section as an overall-scaling factor. As seen in Fig. 15, the classical approximation seems quite accurate. A similar expression was obtained in a previous work.[54]

C. Product distributions

The product distribution in a resonance-mediated reaction should follow the branching ratios for resonance decay, i.e., the ratio of partial widths. We note first the dominance of the HF+D channel over the DF+H channel at low energy in both experiment and theory. Indeed, it is not until $E_C=1$ kcal/mol that the DF+H channel becomes significant. In terms of the resonance picture this behavior is completely understandable. Since the resonance state is highly localized in the FHD collinear arrangement, forming DF+H products would require an internal rotation of HD, which is improbable. In the resonance decay calculations, the flux into the DF+H channel was, in fact, very small. There was no evidence for other mechanisms significantly contributing to the DF+H channel. Specifically, there are no other resonances with the arrangement FDH above between 0 and 1 kcal/mol to feed this channel. The direct, i.e., nonresonant, reaction into the DF+H channel is small for several reasons. An obvious factor is that the higher mass of the D-atom inhibits tunneling. Furthermore, the adiabatic barrier height for this channel is 0.2 kcal/mol higher than for HF+D, which also makes the tunneling smaller. Finally, there is the effect of the steric factors in the reaction. As seen from the classical analysis, the trajectories that react to form HF+D predominately first attack the D-atom, and vice versa. The cone of acceptance interpretation of Johnson *et al.*[55] predicts the DF+H channel should have the higher steric factor since there is a greater range of angles where the D-side of HD is attacked. Because of the migratory character of the trajectories, this argument must be turned around to favor the HF+D channel. Indeed, the low energy classical simulations confirm this.

The Doppler profiles we have measured suggest that the vibrational product distribution, HF(v')+D, is highly dominated by the HF($v'=2$) state at energies below the $v'=3$ threshold. This is unlike higher energy collisions studied here and in previous work, or for the DF(v')+H isotopic channel, which showed a somewhat more ''democratic'' final state distribution. This highly inverted product distribution is consistent with the partial widths of the resonance which predict only 3% decay into the $v'=1$ state and 0.1% decay into the $v'=0$ state. A practical consequence of this distribution is that perhaps the F+HD reaction can be used to create a more efficient chemical laser. In terms of a physical picture, the resonance can be roughly viewed as a state trapped in a well on an adiabatic potential curve that correlates with HF($v'=3$). To decay into the $v'=2$ state, a vibrational transition must occur to the next lowest curve; to decay into the $v'=1$ state a double transition to the next lower curve must occur, etc. If the coupling between the vibrationally adiabatic curves is weak, one expects the transition probability to fall off rapidly with larger quantum number changes.

The rotational product distribution from the experiment is not yet available. However, the calculated rotational distributions are quite interesting. The probability distribution of the states HF($v'=2,j'$) is seen from Fig. 14 to be quite broad and actually peaks at $j'=9$, close to the energetic threshold. Such a distribution argues for a fairly strong bend component in the decay dynamics.

D. Angular distributions

Perhaps the most dramatic observation in the experiment was the rapid variation of the Doppler profile at energies around the position of the resonance. Over an interval of only about 0.2–0.3 kcal/mol, the profiles shifted continuously from backward to sideways and forward distributed. We expect this rapid change to also be manifested in the differential cross section for the HF($v'=2$)+D channel. In the resonance picture, the phase shift of an individual partial wave changes by π in an interval of roughly Γ centered at E_{res}. In the present problem there is negligible direct reaction to interfere with the resonant amplitude. Thus, it is the coherent superposition of resonant amplitudes in many partial waves that combine to determine the differential cross section. From the scattering calculation, we have been able to compute the differential cross section at energies around E_{res}. In Fig. 16, the theoretical differential cross section is seen to go from backward peaked at energies below E_{res}, to more forward and sideways peaked at energies above E_{res}. This is certainly at least in qualitative agreement with the experimental results. A quantitative comparison must wait until the experimental differential cross section is available.

In physical terms, the (3, 0, 0) state should be regarded as a broad resonance since its width (0.15 kcal/mol) is much larger than the rotation constant (0.0051 kcal/mol). This implies that the complex will only rotate a fraction of a period during its lifetime. For example, if we select $J=6$, which shows the maximum of the semiclassical deflection function[56] at $E_C=0.7$ kcal/mol, the rotation period is 1420 fs. Thus, over the course of one resonance lifetime of 109 fs,

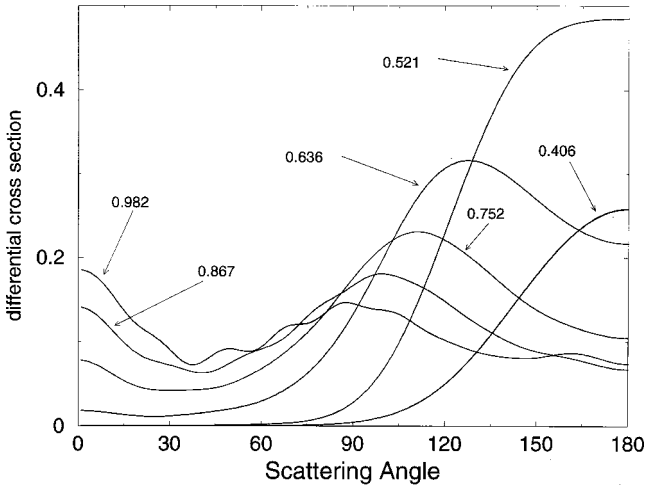

FIG. 16. The differential cross section in square Angstroms obtained from the quantum scattering calculation at six collision energies in the vicinity of the resonance energy. By convention, backward scattering is at 180° and forward scattering is at 0°. The curves are labeled by the collision energy in kcal/mol.

the complex rotates about 28°. This value seems somewhat small in light of the distributions shown in Fig. 16 and the experimental results. However, this sort of simple classical analysis ignores the subtler phase relations between the contributing amplitudes that must underlie the behavior of the quantum angular distribution. A more thorough physical analysis of differential cross section will be deferred to a later work.

E. Critique of the potential function

The combination of highly resolved experimental cross sections and converged quantum mechanical dynamics calculations that we have presented, allows us to comment on the accuracy of the SW-PES. The ability of quantum simulation to reproduce the resonance feature at 0.5 kcal/mol to within 0.1 kcal/mol, is strong evidence for the accuracy of the SW-PES in the collinear portion of the potential surface where the resonance state is built up. Furthermore, the half-width of the step in the excitation function in the range $E_C = 0.3-0.5$ kcal/mol also seems in reasonable agreement with the scattering calculation and with the SQ resonance lifetime. This suggests that the decay coupling, which is largely mediated through the bend, is also reproduced adequately by the SW-PES. Excellent agreement is also observed for the integral cross section for FD+H production. Indeed, as seen in Fig. 4, the computed cross section reproduces the experiment almost exactly from threshold up to 3 kcal/mol of translational energy. The QCT calculations also do well for this reaction. Since we interpret reaction into this channel as a dominantly direct, over the barrier reaction, this agreement suggests that characteristics of the transition state are being correctly modeled. One point of disagreement, as mentioned earlier, is the absolute height of resonance feature. Theory predicts a peak that is about a factor of 2 too large. Since the threshold behavior for the F+HD→FD+H reaction is predicted with great accuracy, we suspect the barrier height may be correct after all, despite the reservations about the neglect of spin–orbit coupling alluded to earlier. However, the theoretical prediction would be too large if the SW-barrier were too narrow and thus gave excess tunneling. Since the reaction coordinate is largely angular, the barrier may be too narrow with respect to γ. Of course, since tunneling is exponentially sensitive to the barrier width, the error may be rather small. From the results available so far, it appears that the spin–orbit correction in the HSW-PES may put the barrier too high to be consistent with experiment. When the experimental product distributions are available, a more sensitive test may be available.

ACKNOWLEDGMENTS

R.T.S. is grateful to Y. T. Lee, S.-H. Lin, and K. Liu for their support and hospitality during his stay at the Institute for Atomic and Molecular Sciences. The work of R.T.S. was partially supported by a grant from the National Science Foundation. The work of K.L., H.S.L., and F.D. was supported by the National Science Council of Taiwan and the Chinese Petroleum Corporation. The work of D.E.M. and D.S. was supported by EPSRC of the United Kingdom.

[1] J. B. Anderson, Adv. Chem. Phys. **41**, 229 (1980).
[2] *Resonances in Electron-Molecule Scattering, van der Waals Complexes, and Reactive Chemical Dynamics*, edited by D. G. Truhlar, ACS Symposium Series Vol. 263 (1984); J. N. L. Connor, W. Jakubetz, and J. Manz, Mol. Phys. **35**, 1301 (1978); J. C. Polanyi and D. C. Tardy, J. Chem. Phys. **51**, 5717 (1969). J. H. Parker and G. C. Pimintel, *ibid.* **51**, 91 (1969).
[3] D. M. Neumark, A. M. Wodtke, G. N. Robinson, C. C. Hayden, and Y. T. Lee, J. Chem. Phys. **82**, 3045 (1985); D. M. Neumark, A. M. Wodtke, G. N. Robinson, C. C. Hayden, K. Shobatake, R. K. Sparks, T. P. Schafer, and Y. T. Lee, *ibid.* **82**, 3067 (1985).
[4] M. Faubel, S. Schlemmer, F. Sondermann, U. Tappe, and J. P. Toennies, J. Chem. Phys. **94**, 4676 (1991); M. Faubel, L. Rusin, S. Schlemmer, F. Sondermann, U. Tappe, and J. P. Toennies, *ibid.* **101**, 2106 (1994); G. Dharmasena, K. Copeland, J. H. Young, R. A. Lasell, T. R. Phillips, G. A. Parker, and M. Keil, J. Phys. Chem. **101**, 6429 (1997); J. Chem. Phys. **106**, 9950 (1997).
[5] F. J. Aoiz, L. Banares, V. J. Herrero, V. Saez Ravanos, K. Stark, and H.-J. Werner, J. Phys. Chem. **98**, 10665 (1994); J. Chem. Phys. **102**, 9248 (1994).
[6] J. F. Castillo, D. E. Manolopoulos, K. Stark, and H.-J. Werner, J. Chem. Phys. **104**, 6531 (1996).
[7] G. S. Schatz, Annu. Rev. Phys. Chem. **39**, 317 (1988).
[8] W. H. Miller and J. Z. H. Zhang, J. Phys. Chem. **95**, 12 (1991).
[9] H. Feshbach, *Theoretical Nuclear Physics* (Wiley, New York, 1992).
[10] D. A. Kliner, D. E. Adelman, and R. N. Zare, J. Chem. Phys. **94**, 1069 (1991).
[11] J. Z. H. Zhang and W. H. Miller, J. Chem. Phys. **91**, 1528 (1989).
[12] S. E. Bradforth, D. W. Arnold, D. M. Neumark, and D. E. Manolopoulos, J. Chem. Phys. **99**, 6345 (1993); A. Weaver and D. M. Neumark, Faraday Discuss. Chem. Soc. **91**, 5 (1991).
[13] D. E. Manolopoulos, K. Stark, H.-J. Werner, D. W. Arnold, S. E. Bradforth, and D. M. Neumark, Science **262**, 1852 (1993).
[14] R. T. Skodje, R. Sadeghi, and J. L. Krause, J. Chem. Soc., Faraday Trans. **93**, 765 (1997).
[15] I. M. Waller, T. N. Kitsopoulos, and D. M. Neumark, J. Phys. Chem. **94**, 2240 (1990).
[16] S.-F. Wu, R. B. Johnson, and R. D. Levine, Mol. Phys. **25**, 839 (1973).
[17] G. S. Schatz, J. M. Bowman, and A. Kuppermann, J. Chem. Phys. **63**, 674 (1975); **63**, 685 (1975).
[18] D. G. Truhlar and A. Kuppermann, J. Chem. Phys. **56**, 2232 (1972); J. M. Launay and M. LeDourneuf, J. Phys. B **15**, L455 (1982); J. M. Launay and B. Lepetit, Chem. Phys. Lett. **144**, 346 (1988).
[19] K. Stark and H.-J. Werner, J. Chem. Phys. **104**, 6515 (1996).
[20] F. J. Aoiz, L. Banares, V. J. Herrero, V. Saez Rabanos, K. Stark, I. Tanarro, and H.-J. Werner, Chem. Phys. Lett. **262**, 175 (1996); F. J. Aoiz,

L. Banares, V. J. Herrero, V. Saez Rabanos, K. Stark, and H.-J. Werner, J. Chem. Phys. **102**, 9248 (1995).
[21] J. F. Castillo, B. Hartke, H.-J. Werner, F. J. Aoiz, L. Banares, and B. Martinez-Haya, J. Chem. Phys. **109**, 7224 (1998).
[22] J. F. Castillo and D. E. Manolopoulos, Faraday Discuss. **110**, 119 (1998).
[23] B. Hartke and H.-J. Werner, Chem. Phys. Lett. **280**, 430 (1997); E. Rosenman, Z. Hockman-Kowal, A. Persky, and M. Baer, *ibid.* **257**, 421 (1996); P. Honvaunt and J. M. Launey, *ibid.* **303**, 657 (1999); M. Baer, *ibid.* **312**, 203 (1999).
[24] C. L. Russell and D. E. Manolopoulos, Chem. Phys. Lett. **223**, 215 (1996).
[25] R. E. Wyatt, J. F. McNutt, and M. J. Redmon, Ber. Bunsenges. Phys. Chem. **86**, 437 (1982); T. C. Thompson and D. G. Truhlar, J. Phys. Chem. **88**, 210 (1984); J. D. Kress, Z. Bacic, G. A. Parker, and R. T. Pack, Chem. Phys. Lett. **157**, 484 (1989).
[26] T. Takayanagi and Y. Kurosaki, J. Chem. Phys. **109**, 8929 (1998).
[27] Y.-T. Hsu, J.-H. Wang, and K. Liu, J. Chem. Phys. **107**, 2351 (1997); S.-H. Lee and K. Liu, Chem. Phys. Lett. **290**, 323 (1998).
[28] W. B. Chapman, B. W. Blackmon, S. Nizkorodov, and D. J. Nesbitt, J. Chem. Phys. **109**, 9306 (1998).
[29] M. H. Alexander, H.-J. Werner, and D. E. Manolopoulos, J. Chem. Phys. **109**, 5710 (1998).
[30] S.-H. Lee and K. Liu, J. Chem. Phys. **111**, 6253 (1999).
[31] V. Aquilanti, R. Candori, D. Cappelletti, E. Luzzatti, and F. Pirani, Chem. Phys. **145**, 293 (1990).
[32] S.-H. Lee, F. Dong, and K. Liu (unpublished).
[33] D. E. Manolopoulos, J. Chem. Soc., Faraday Trans. **93**, 673 (1997), and references therein.
[34] D. Skouteris, D. E. Manolopoulos, W. Bian, H.-J. Werner, L.-H. Lai, and K. Liu, Science **286**, 1713 (1999).
[35] Y.-T. Hsu and K. Liu, J. Chem. Phys. **107**, 1664 (1997).
[36] S.-H. Lee and K. Liu, J. Phys. Chem. **102**, 8637 (1998).
[37] J. M. Mestdagh, J. P. Visticont, and A. G. Suits, in *The Dynamics and Kinetics of Small Radicals*, edited by K. Liu and A. Wagner (World Scientific, Singapore, 1995), Vol. II, Chap. 6.
[38] A closer examination reveals that the backward hemisphere is somewhat smaller than the forward component. Nevertheless, the main point here is the drastic change in the appearance of the ‖-Doppler profiles as a function of energy.
[39] The parameters used in the present calculations were the same as those used in Ref. 22 except for the helicity truncation parameter, $k_{\max}$, which was reduced from 4 to 3 to save computer time. This reduction of $k_{\max}$ was found to change the computed integral cross sections by less than 5% at each of the two collision energies ($E_C = 1.35$ and 1.98 kcal/mol) for which the calculations in Ref. 22 were performed.
[40] R. T. Skodje, J. Chem. Phys. **95**, 7234 (1991).
[41] R. T. Skodje, Annu. Rev. Phys. Chem. **44**, 145 (1993).
[42] M. Gutzwiller, *Chaos in Classical and Quantum Mechanics* (Springer, New York, 1990); I. Burkhardt and P. Gaspard, J. Chem. Phys. **100**, 6395 (1994).
[43] E. Pollak and M. S. Child, Chem. Phys. **63**, 23 (1981).
[44] R. Sadeghi and R. T. Skodje, J. Chem. Phys. **102**, 193 (1995).
[45] R. T. Skodje, R. Sadeghi, J. R. Krause, and H. Koppel, J. Chem. Phys. **101**, 1725 (1994).
[46] G. S. Schatz and A. Kuppermann, J. Chem. Phys. **65**, 4642 (1975).
[47] R. Sadeghi and R. T. Skodje, J. Chem. Phys. **98**, 9208 (1993); **99**, 5126 (1993); **102**, 193 (1995); R. Sadeghi and R. T. Skodje, Phys. Rev. A **52**, 1996 (1995); J. Chem. Phys. **105**, 7504 (1996); R. Sadeghi, S. R. Gwaltney, J. L. Krause, R. T. Skodje, and P. W. Weber, *ibid.* **107**, 6570 (1997); R. T. Skodje, R. Sadeghi, and J. L. Krause, Chem. Phys. **240**, 129 (1999).
[48] B. Jackson, M. Person, and B. D. Kay, J. Chem. Phys. **100**, 7687 (1994); A. Isele, C. Meier, V. Engel, N. Fahrer, and Ch. Schlier, *ibid.* **101**, 5919 (1994); S. Mahapatra and N. Sathyamurthy, *ibid.* **102**, 6057 (1995); A. J. C. Varandas and H. G. Yu, Chem. Phys. Lett. **209**, 31 (1996).
[49] J. R. Taylor, *Scattering Theory*, Chap. 20.
[50] S. L. Mielke, G. C. Lynch, D. W. Schwenke, and D. G. Truhlar, Chem. Phys. Lett. **217**, 173 (1994).
[51] G. S. Schatz, Science **262**, 1828 (1993).
[52] R. H. Bisseling, R. Kosloff, J. Manz, F. Mrugala, J. Romelt, and G. Weichselbaumer, J. Chem. Phys. **86**, 2626 (1987).
[53] J. M. Bowman, J. Phys. Chem. **95**, 4960 (1991).
[54] G. C. Schatz, D. Sokolovsky, and J. N. L. Connor, Discuss. Faraday Soc. **91**, 17 (1991); J. Chem. Phys. **94**, 4311 (1991).
[55] J. W. Johnson, H. Kornweitz, I. Schechter, A. Persky, B. Katz, R. Bersohn, and R. D. Levine, J. Chem. Phys. **94**, 2749 (1991).
[56] E. F. Hayes and R. B. Walker, J. Phys. Chem. **88**, 3318 (1984).